INL/RPT-24-80355

Advanced Reactor Technologies

Summary Report Of The FY24 DOE Contributions To The GIF VHTR CMVB

M3AT-24IN0603011

SEPTEMBER 2024

Sinan Okyay,
Joshua J. Cogliati,
Victor C. Leite,
David A. Reger,
Paolo Balestra, and
Gerhard Strydom

Idaho National Laboratory

Idaho National Laboratory

INL/RPT-24-80355

Summary Report Of The FY24 DOE Contributions To The GIF VHTR CMVB

M3AT-24IN0603011

Sinan Okyay,
Joshua J. Cogliati,
Victor C. Leite,
David A. Reger,
Paolo Balestra, and
Gerhard Strydom
Idaho National Laboratory

September 2024

Idaho National Laboratory
INL ART Program
Idaho Falls, Idaho 83415

http://www.inl.gov

Prepared for the
U.S. Department of Energy
Office of Nuclear Energy
Under DOE Idaho Operations Office
Contract DE-AC07-05ID14517

Page intentionally left blank

INL ART Program

Summary Report of the FY24 DOE Contributions to the GIF VHTR CMVB

INL/RPT-24-80355

September 2024

Technical Reviewer: (Confirmation of mathematical accuracy, and correctness of data and appropriateness of assumptions.)

M. Turkmen — 8/30/2024

Mehmet Turkmen — Date
Nuclear Engineer

Approved by:

8/22/2024

Michael E. Davenport — Date
ART Project Manager

Travis Mitchell — 8/22/2024

Travis R. Mitchell — Date
ART Program Manager

8/22/2024

Michelle T. Sharp — Date
INL Quality Assurance

Page intentionally left blank

ABSTRACT

The Generation-IV Forum (GIF) Very-High-Temperature Reactor-Computational Methods Validation and Benchmark (VHTR-CMVB) Initiative, involving organizations from Korea Atomic Energy Research Institute (KAERI) (South Korea), Institute of Nuclear and New Energy Technology of Tsinghua University (INET) (China), U.S. Department of Energy (DOE) (U.S.), Joint Research Centre (JRC) (Europe), and Japan Atomic Energy Agency (JAEA) (Japan), is dedicated to the verification and validation of tools for High-Temperature Gas-Cooled Reactors (HTGRs) analyses, using data shared by Computational Methods Validation and Benchmark (CMVB) signatories. For Fiscal Year 2024, the DOE CMVB has committed to several critical activities. Under work package 1, led by the United States, the integration of the High Temperature Gas Cooled Reactor - Pebble-Bed Module (HTR-PM) Phenomena Identification and Ranking Table (PIRT) into the comparative PIRT is progressing, with a new draft of the comparison tables issued earlier this year and currently being utilized by INET for their contribution. Neutronic validation efforts under work package 3 include the preparation of the burnup analysis benchmark, preliminary calculations, and the development of reference models and results. In work package 2, a validation exercise for hot gas mixing in the lower plenum of HTR-PM is in progress, using experimental data from INET to validate modeling approaches. A model of the experimental facility has been developed using StarCCM+, with initial calculations slated for presentation at the GIF CMVB meeting this fall. Another work package 2 activity focuses on validating numerical models for air-cooled Reactor Cavity Cooling System (RCCS) with experimental data from the Wisconsin Madison RCCS facility. A high-fidelity model, developed using NekRS, is currently being validated with available data from a low-power forced-convection test. These efforts are aimed at enhancing and confirming the accuracy of HTGR analysis tools, ensuring their alignment with experimental data and regulatory requirements.

Page intentionally left blank

CONTENTS

FIGURES

TABLES

Page intentionally left blank

ACRONYMS

ANL	Argonne National Laboratory
ATR	Advanced Test Reactor
CAD	Computer-aided design
CFD	Computational Fluid Dynamics
CMVB	Computational Methods Validation and Benchmark
DNS	Direct Numerical Simulation
DOE	U.S. Department of Energy
GA-MHTGR	General Atomics' Modular High-Temperature Gas Reactor
GIF	Generation-IV Forum
HTGR	High-Temperature Gas-Cooled Reactor
HTR-PM	High Temperature Gas Cooled Reactor - Pebble-Bed Module
INET	Institute of Nuclear and New Energy Technology of Tsinghua University
INL	Idaho National Laboratory
JAEA	Japan Atomic Energy Agency
JRC	Joint Research Centre
KAERI	Korea Atomic Energy Research Institute
LES	Large Eddy Simulations
MCNP	Monte Carlo N-Particle
MFR	Mass Flow Rate
MOOSE	Multiphysics Object-Oriented Simulation Environment

NSTF	Natural Convection Shutdown Heat Removal Test Facility
PIRT	Phenomena Identification and Ranking Table
RANS	Reynolds-Averaged Navier Stokes
RCCS	Reactor Cavity Cooling System
RPV	Reactor Pressure Vessel
TRISO	TRi-structural ISOtropic
UW-Madison	The University of Wisconsin-Madison
VHTR	Very-High-Temperature Reactor
VHTR-CMVB	Very-High-Temperature Reactor-Computational Methods Validation and Benchmark

Page intentionally left blank

Summary Report of the FY24 DOE Contributions to the GIF VHTR CMVB

M3AT-24IN0603011

1. PROGRESS ON PIRT REVIEW AND COMPARISON TASK

One of the primary challenges in designing and licensing a High-Temperature Gas-Cooled Reactor (HTGR) is ensuring that computational tools and methods can be reliably used to meet design and safety objectives under key scenarios. This process begins with creating a Phenomena Identification and Ranking Table (PIRT), which helps in developing a validation matrix. Initially, scenarios that challenge the system are identified and experts assess key phenomena within these scenarios, categorizing them as high, medium, or low based on their importance and the current state of knowledge. This prioritization informs the validation matrix, focusing on the data or experiments needed to address critical phenomena. To ensure data adequacy or identify additional needs, the process involves defining and prioritizing experiments essential for licensing, particularly those impacting safety or lacking sufficient knowledge. In Task 1.1 of work package 1 of the Very-High-Temperature Reactor-Computational Methods Validation and Benchmark (VHTR-CMVB) Program, participants are tasked with updating PIRTs and comparing them across different organizations. A comparison table template has been created and currently under review by the participants. Currently, Institute of Nuclear and New Energy Technology of Tsinghua University (INET) is incorporating the importance and level of knowledge developed during the High Temperature Gas Cooled Reactor - Pebble-Bed Module (HTR-PM) licensing process. An example of the reviewed tables used for this purpose is shown in Figure 1. Existing PIRTs may be outdated due to new experiments and varying expert opinions, so this review and update process is crucial for improving the overall understanding of Very-High-Temperature Reactor (VHTR) scenarios and phenomena.

Table 3: Combined PIRT table for thermal fluids phenomena during normal operations.

ID No.	Characteristics	Comments	FOM	R. Type	Importance - Knowledge Level US	CN	JP	EU	KR
1	Core coolant bypass flow.	Determines active core cooling; affects $T_{fuel,max}$. …	Fuel time and temperature, fuel failure fraction.	PBR	H-L				
				PMR	H-L				
2	Core flow distribution, flow in active core.	Determines fuel operating temperatures. Assumes known bypass flows. …	//	PBR	H-M				
				PMR	H-M				
3	Core flow distribution changes due to temperature gradients.	Some effect on fuel operating temperatures. Active core flow. Large delta T from inlet to outlet. Gradients different from LWRs. …	//	PBR	M-M				
				PMR	M-M				
4	Core flow distribution changes due to graphite irradiation.	Some effect on fuel operating temperatures. …	//	PMR	M-L				
5	Core flow distribution changes due to core barrel geometry changes.	Some effect on fuel operating temperatures. Wouldn't apply to case where inlet flow enters through reflectors. …	//	PBR	M-M				
				PMR	M-M				
6	Core flow distribution due to core block stability.	Bypass leakage flow induce vibrations in the blocks. …	//	PMR	M-M				

Figure 1. Cover page of the PIRT consolidation document (left) and an example comparison table (right).

2. NEUTRONIC VALIDATION BENCHMARK USING AGR-1/2 DATA

2.1. AGR-1 GIF Benchmark

The Idaho National Laboratory (INL) document "AGR-1 Depletion Benchmark" [1] has been converted and updated for use with the Generation-IV Forum (GIF) Neutronic validation benchmark. The considered update has included formatting, adding experimental data for comparison with results, and creating a results spreadsheet.

2.2. AGR-1 Models

As part of checking the AGR-1 GIF Benchmark document and for future use in model and code-to-code comparisons, two different Monte Carlo N-Particle (MCNP)[2] models of the AGR-1 experiment have been created. The simpler model homogenizes the compact materials, including the graphite matrix and TRi-structural ISOtropic (TRISO) particles, to one single material, as can be seen in Figure 2. The alternative model includes TRISO particles modeled inside of an MCNP lattice, as can be seen in Figure 3.

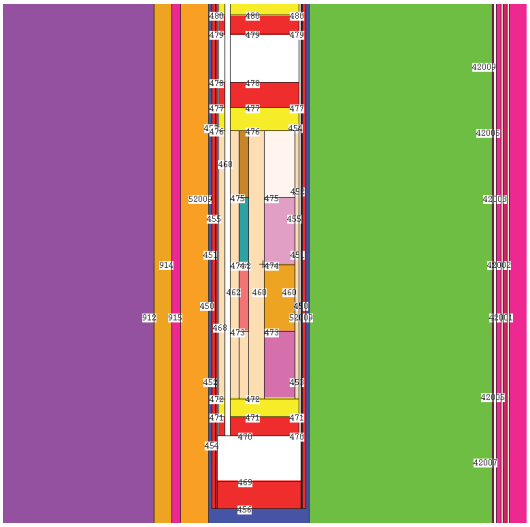

Figure 2. Axial view of capsule with homogeneous compacts for AGR-1.

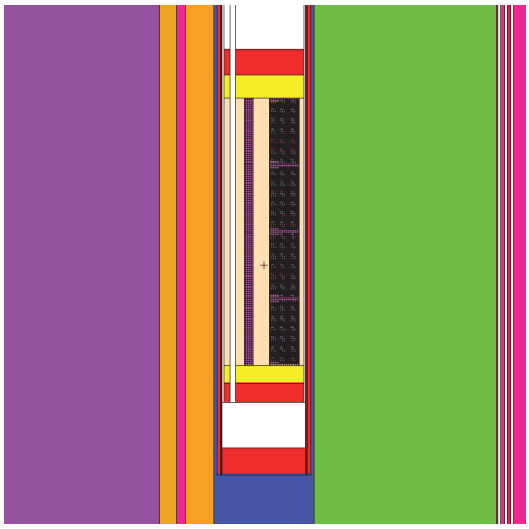

Figure 3. Axial view of capsule with TRISO particles for AGR-1.

2.3. AGR-1 Results And Comparison To Experimental Results

Several radioactive nuclides were measured after the AGR-1 experiment was removed from Advanced Test Reactor (ATR). The grams experimentally measured and the calculated values for all the capsules combined are listed in Table 1. The final experimental values and the calculated path to them are shown in Figures 4, 5, and 6. The data were also calculated for individual compacts and the results for Capsule 3 Stack 3 Compact 4 are in Table 2.

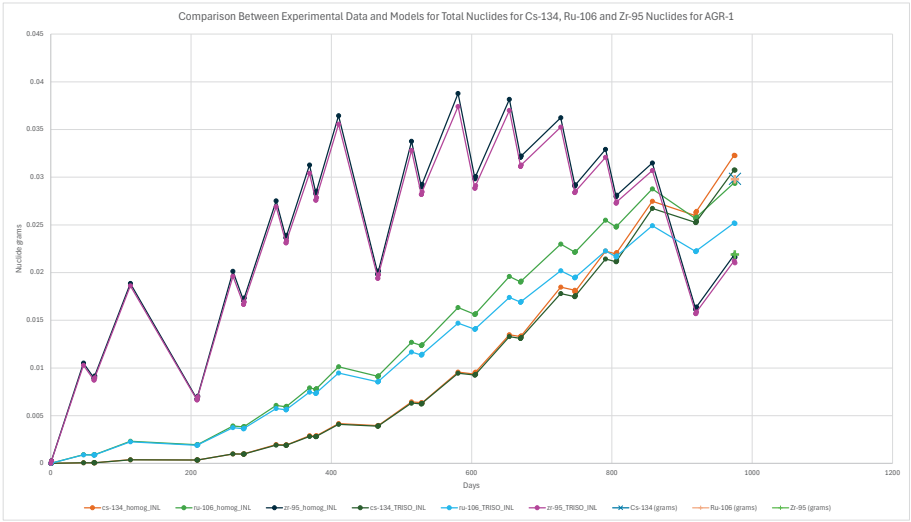

Figure 5. Comparison between Cs-134, Ru-106, and Zr-95 nuclides from AGR-1 model and experimental results.

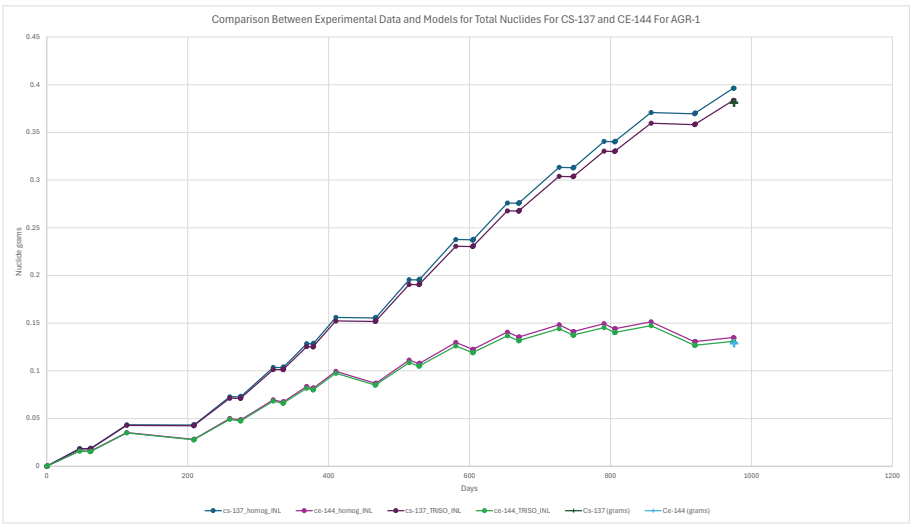

Figure 4. Comparison between Cs-137 and Ce-144 from AGR-1 model and experimental results.

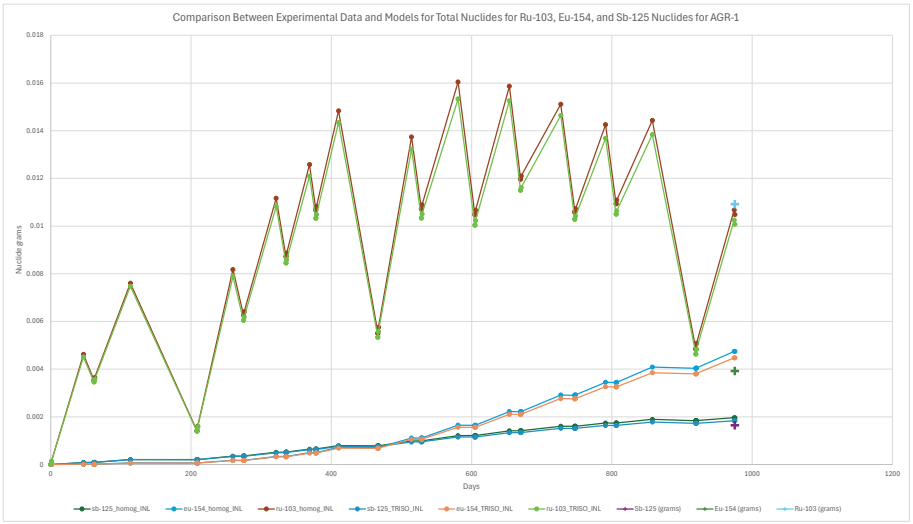

Figure 6. Comparison between Ru-103, Eu-154, and Sb-125 nuclides from AGR-1 model and experimental results.

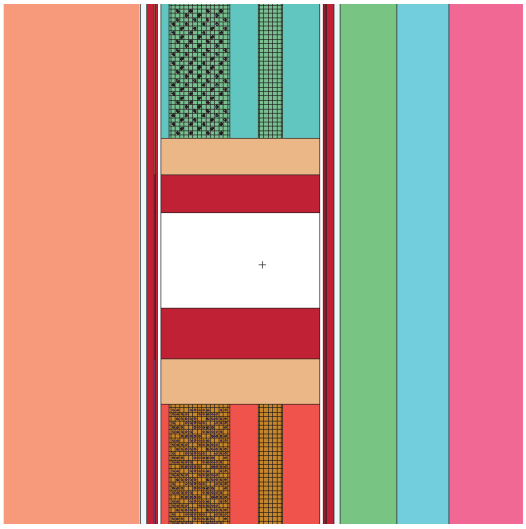

Figure 7. Axial view of capsule with TRISO particles for AGR-2

Table 1. Comparison of AGR-1 nuclides at end of cycles between MCNP model and Experimental data.

Nuclide	Experimental (gm)	Homogeneous Model	TRISO Model
Cs-137	3.81E-01	3.96E-01	3.84E-01
Cs-134	2.98E-02	3.23E-02	3.07E-02
Sb-125	1.60E-03	2.00E-03	1.80E-03
Eu-154	3.90E-03	4.70E-03	4.50E-03
Ce-144	1.29E-01	1.35E-01	1.31E-01
Ru-106	2.98E-02	2.94E-02	2.52E-02
Zr-95	2.19E-02	2.16E-02	2.10E-02
Ru-103	1.09E-02	1.05E-02	1.01E-02

Table 2. Comparison of AGR-1 Nuclides in Capsule 3 Stack 3 Compact 4 at end of cycles between MCNP Model and Experimental Data

Nuclide	Experimental (gm)	Homogeneous Model	TRISO Model
Cs-137	6.2720E-03	5.7330E-03	5.6160E-03
Cs-134	6.2312E-04	4.9150E-04	4.7173E-04
Sb-125	2.6323E-05	2.8640E-05	2.7753E-05
Eu-154	7.5762E-05	7.4560E-05	7.1220E-05
Ce-144	1.8327E-03	1.9290E-03	1.9443E-03
Ru-106	5.3625E-04	4.3830E-04	3.9838E-04
Zr-95	2.6152E-04	2.9810E-04	3.0985E-04
Ru-103	1.5562E-04	1.4240E-04	1.5110E-04
Ce-141	1.5051E-04	2.1460E-04	2.2090E-04

2.4. AGR-2 Data Gathering

AGR-2 has many notable differences compared to AGR-1. The documentation for this is currently located in multiple INL documents including drawings, internal reports and external reports. This has been collected into a single document for use in benchmarking. The most notable difference is the use of uranium oxide in some of the capsules compared to AGR-1, which are all uranium oxy-carbide (UCO). The TRISO particles used have somewhat different typical dimensions compared to the AGR-1 versions, and have different numbers of particles per compact and different enrichments compared to the AGR-1 versions. These changes have been documented and will be combined into a new AGR-1 and AGR-2 benchmark description. As well, an AGR-2 MCNP model using this data has been created and was used for Figure 7.

3. CFD VALIDATION USING WISCONSIN MADISON AIR-COOLED RCCS EXPERIMENTAL FACILITY

HTGRs have attracted interest thanks to their exceptional passive safety systems and ability to provide process heat, as outlined by the U.S. Department of Energy (DOE) [3]. HTGR passive safety systems, which often rely on fundamental principles of nature, do not employ compressors, pumps, or other active components during accident scenarios. This means minimal human intervention is required to operate them under accident conditions [4]. These reactor concepts rely on a Reactor Cavity Cooling System (RCCS) to carry out decay heat over long-term transients from the Reactor Pressure Vessel (RPV) in accident scenarios.

Many applications in nuclear reactors (including RCCS designs) are governed by the interaction of various physical processes (such as fluid flow, heat transfer, and neutron transport). Vendors must understand these interactions to ensure these systems meet their design specifications, particularly during accidents. Vendors often utilize the numerical tools to test and optimize their designs. The numerical tools offer a cost-effective and fast-paced method to improve the designs. Hence, numerical tools for producing accurate simulations are in high demand within the industrial community.

Recent advancements in the thermal-hydraulic characterization of the RCCS have been driven by numerous experimental and numerical studies, as highlighted in works such as References [4–11]. An essential contribution to this field has been made by Argonne National Laboratory (ANL) through their Natural Convection Shutdown Heat Removal Test Facility (NSTF). This facility has provided high-quality experimental and numerical data for the RCCS designed for General Atomics' Modular High-Temperature Gas Reactor (GA-MHTGR) [5–7, 11].

The NSTF stands out from other experimental studies due to its larger scale, being a half-scale model of the original GA-MHTGR design. This highlights the significance of the experimental data obtained from the facility [5]. Moreover, there are multiple experimental studies performed on a smaller scale compared to NSTF, such as Reference [10] employing a RCCS designed for the PMR200 and [4] using the GA-MHTGR RCCS design. Both studies provide experimental data under various conditions on a quarter scale of different RCCS designs.

The following studies use system-level thermal hydraulics codes for predicting temperature distribution under different heating conditions for RCCSs [7, 9]. Computational Fluid Dynamics (CFD) tools have been employed to understand the thermal-hydraulic characteristics and optimize the existing design of the RCCSs [11, 12]. The study by Hu et al. states that atmospheric conditions can affect the thermal-hydraulic characteristics of the system [12]. Reference [11] provides some prior CFD analysis for the NSTF facility and shows the effect of various geometric configurations on the thermal-hydraulic characteristics. Moreover, Freile [8] employs CFD tools to enhance the performance of system-level thermal-hydraulic analysis codes. The literature does contain high-fidelity CFD simulations for partial geometries of RCCS, including Large Eddy Simulations (LES) of riser ducts [13]. However, to the best of our knowledge, a notable gap exists in the literature concerning high-fidelity simulations of the full complete model of RCCS.

This study focuses on a specific air-cooled RCCS designed for GA-MHTGR. The University of Wisconsin-Madison (UW-Madison) conducted experiments on the quarter-scaled version of the original design [4]. The present work has two aims to contribute to the thermal-hydraulic validation of the RCCS:

- To provide high-fidelity CFD results on the RCCS experiments conducted at UW-Madison
- To contribute to establishing a benchmark for the UW-Madison RCCS, measuring and comparing the performance of the various numerical tools in RCCS scenarios.

The following sections will provide information on the UW-Madison RCCS facility and the conducted experiments in the facility. Then, the modeling strategy for the simulations will be explained, followed by the validation of the numerical tool. Lastly, the preliminary results on the RCCS geometry will be presented.

3.1. RCCS Test Facility

The GA-MHTGR is designed for a 450 MW_{th} output. The RCCS for this system uses air to remove heat and consists of 227 rectangular ducts. It is designed to remove 700 kW during normal operation and a maximum of $1.5MW$ during accident conditions (low-flow conditions). The UW-Madison quarter-scale RCCS facility, overall 13 meters tall, is constructed of six riser ducts representing a 10° slice of the full-scale GA-MHTGR RCCS design. The original and scaled facility designs are shown in Figure 8.

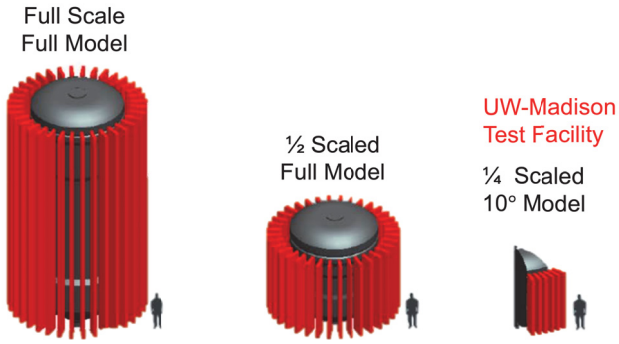

Figure 8. Scaled version of air-cooled RCCS for GA-MHTGR [4].

The experiment consisted of three main components: the inlet plenum, heated cavity, and outlet plenum and exhaust ducts (see Figure 9). The inlet plenum is the entry point for air drawn from the environment by the circulator in the RCCS. Within the heated cavity, electrical resistance heaters (mounted on the walls of the heated cavity) simulate the RPV and emit heat to the six riser ducts. Additionally, the air inside of the heated cavity participates in the heat transfer between riser ducts and heaters. The air is heated by the heaters and transfers heat to riser ducts via convection. Finally, the outlet plenum serves as a mixing space prior to the heated air being released back into the environment via a pair of exhaust ducts. The orange arrows in Figure 9 indicate the airflow direction inside the RCCS.

Two types of heat transfer regimes were tested in this facility: forced and natural convection tests. Natural convection tests were conducted with both uniform and asymmetric flux in order to investigate the effect of power shape, whereas the forced convection tests were conducted using only a uniform flux profile. Each type of test was run at two different power levels and repeated two times to analyze repeatability. Only one of the four tests, conducted under the uniform flux scenario at low power, showed unstable behavior (i.e., flow reversal present in the exhaust ducts). Table 3 provides a summary of the experiments conducted. Out of the 12 successful tests, the first four were performed under forced circulation conditions, the next four utilized natural convection with uniform heating, and the final four employed natural convection with non-uniform heating. Notably, one of the tests with natural convection and uniform heating experienced instability. Furthermore, all four tests involving natural convection with non-uniform heating exhibited instability. This

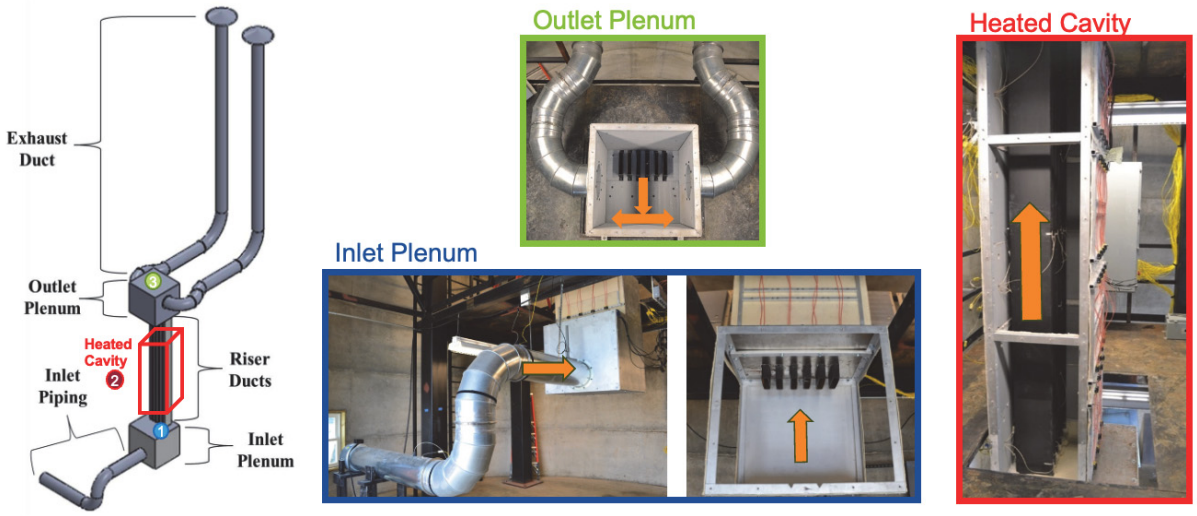

Figure 9. Facility overview (images taken from [4]).

instability is attributed to external weather conditions affecting the facility and the asymmetric heating of different channels, which contribute to localized instability.

Table 3. Experiment summary.

Type	Case	# of Experiments	Instability
Forced Convection	Forced Flow	4 (2 Power Levels, 2 Repeat)	No (All Experiments)
Natural Convection	Uniform Flux	4 (2 Power Levels, 2 Repeat)	Yes (1 of 4 Experiments)
	Asymmetric Flux	4 (2 Power Levels, 2 Repeat)	Yes (All Experiments)

Instrumentation is installed throughout the facility to control power and measure temperature and velocity at specified locations as shown in Figure 10. Electrical heaters are mounted on the walls of the heated cavity to supply heat to the system. To ensure the characterization of heat removal from the RCCS, temperature measurements are taken at various points. Velocity measurements are obtained from the system entrance due to temperature restrictions on the velocity sensors. The velocity data is used to ensure the consistent flow rates on the riser entrances. The schematic location of the instrumentation can be seen in Figure 10. The temperature data will be compared with the simulation results at various locations to validate the numerical results.

3.2. Modeling Strategy Of UW-Madison RCCS

The experiments will be simulated in three stages, starting with simpler scenarios and advancing to more complex ones. Initially, the focus will be on forced convection cases, which will help validate the numerical model using less intricate physics. Following this, forced convection cases will focus on validating the thermal-hydraulic performance of the numerical model, including radiative heat transfer. Then, natural convection will be simulated with the existing model. The first natural convection tests reflect the nominal conditions (based on uniform flux) such as operation or low-flow conditions. The last tests will focus on accident scenarios in which asymmetric heat flux will be analyzed to observe the nonuniform heating effects on the RCCS.

The proposed modeling strategy is illustrated in Figure 11. The setup will be explained in two separate parts: the heated cavity and the cooling system. The heated cavity section aims to simulate the transport

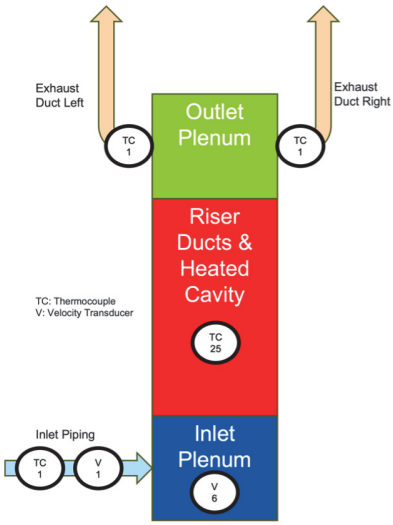

Figure 10. UW-Madison RCCS instrumentation, where the numbers represent the number of measurement devices in the section.

of heat from the heaters (representing the reactor pressure vessel) to the riser ducts. The cooling system facilitates the removal of heat from the system using the principles of forced or natural convection. The heated cavity and cooling system have separate fluid flows, and their fluids do not mix. The fluid flow inside the heated cavity plays an important role in heat transfer but has no direct effect on the fluid flow inside the cooling system. Therefore, modeling the heated cavity and cooling system separately improves the stability of each system. The heated cavity and cooling system are coupled through the walls of the riser ducts where the energy variable is transferred between the systems.

The difference between the natural and forced convection tests is the dependency of energy and momentum variables on each other. Forced convection cases will start solving the heat transfer in the heated cavity, and the energy variable (temperature or heat flux) on the wall will be sent to the cooling system to use as a boundary condition for fluid flow. In natural convection cases, energy and momentum variables are strongly interdependent, requiring a continuous exchange of these variables during the simulation. The energy variable (such as temperature or heat flux) is transferred to the cooling system, and the resulting changes in these variable is then fed back into the heated cavity. Figure 11 is colored by the numerical tools employed to solve the corresponding system, which will be explained in Section 3.3.

The heated cavity is crucial to the air-cooled RCCS facility, serving as a thermal enclosure that transfers heat from the heaters to the six riser ducts while minimizing heat losses to the environment. Heat transfer occurs primarily by radiation and secondarily by convection. Additionally, conduction occurs between the heaters and the frame of the heated cavity as the heaters are mounted within the cavity frame. Figure 12 presents a heat diagram of the heated cavity system. It should be noted that, in Figure Figure 12, the heat transferred to the frame is lost to the environment.

Figure 13 shows the numerical model alongside a sketch of the experimental facility. The study's initial focus is to model the forced convection cases. The initial model will ensure accurate modeling of the inlet plenum, riser ducts, and outlet plenum. Therefore, this model does not yet include the exhaust ducts or all the inlet piping. The natural convection cases will have different boundary conditions for the velocity since the buoyancy pressure drop dictates the mass flow rate.

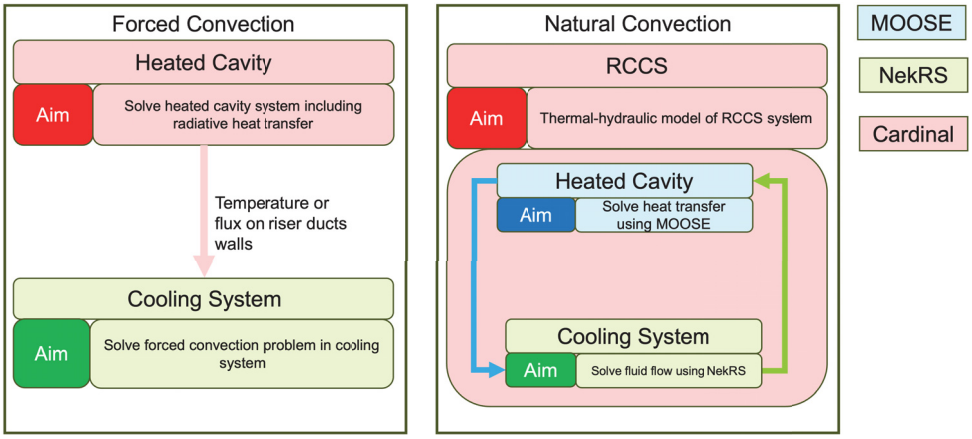

Figure 11. Modeling strategy for the RCCS scenarios.

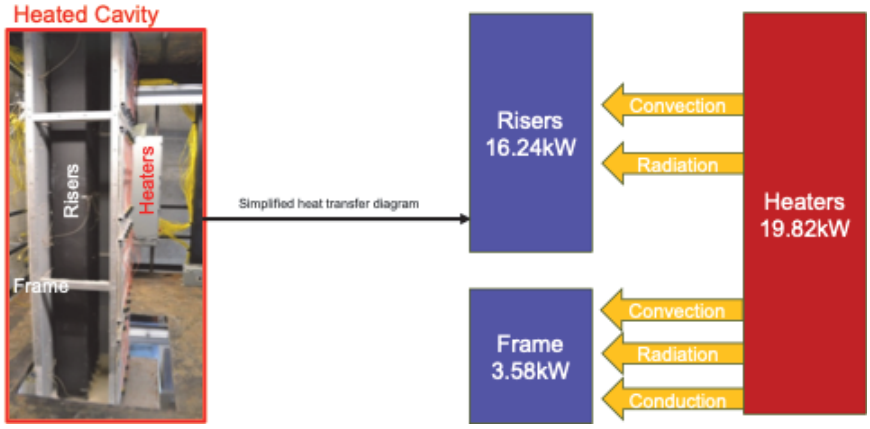

Figure 12. The heated cavity heat transfer diagram.

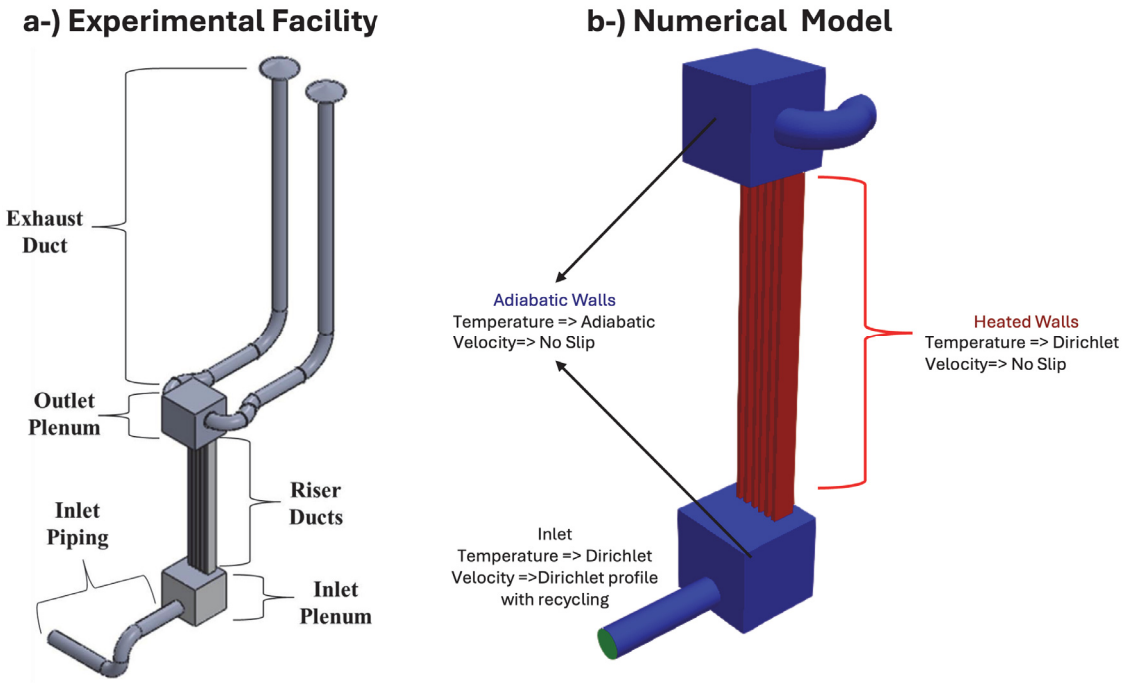

Figure 13. RCCS cooling system boundary conditions.

3.3. Validation Of The Numerical Tools And Methodology

This section will present the validation and verification for the numerical tools. There are three main numerical tools employed in this study to perform thermal-hydraulic analysis of the experimental RCCS facility.

- The Multiphysics Object-Oriented Simulation Environment (MOOSE) is a simulation environment for performing multiscale, multiphysics simulations [14] developed by INL. The MOOSE implementation primarily relies on the finite-element method, which solves equations by employing a set of shape functions to obtain the solution for a system of equations [15]. The MOOSE tools are employed to solve heat transfer in the heated cavity system.
- NekRS, an open-source code for solving CFD problems [16]. NekRS was developed by ANL for simulating transitional and turbulent flows in complex geometries [16]. It employs the spectral element method, a high-order weighted residual technique that combines the geometric flexibility of finite elements with the rapid convergence and computational efficiency of global spectral methods [17]. NekRS will be used to create a high-fidelity simulation of the airflow in the RCCS cooling system.
- Cardinal is an open-source application built on MOOSE [18]. It integrates the NekRS spectral element CFD code into the MOOSE framework. Cardinal utilizes MOOSEs versatile multiapplication and data transfer systems, independent of specific physics or geometry, to facilitate high-resolution multiphysics feedback coupling with other MOOSE-based tools. Cardinal will be used to transfer energy variables between NekRS and the MOOSE framework for natural convection cases.

3.3.1. Heated Cavity

MOOSE was used to simulate the system presented in Figure 12. Radiation and conduction were modeled by leveraging the respective MOOSE modules to solve the heat balance equations.

$$\dot{q} = -\nabla \cdot (k \nabla T) \tag{1}$$

where T is temperature, k is the thermal conductivity, and $\dot{q}$ is a heat source. The total power is distributed to each heater as a uniform volumetric heat source. Convection, on the other hand, was modeled simply as convective boundary conditions, which imply a Robin boundary condition at the specified location. Below, the heat transfer coefficients are summarized for the thermal model. As a first approximation, a correlation valid for tall cavities was utilized to calculate the heat transfer coefficient for the cavity interior [19]. Since the heated cavity is an enclosed box, the heat removed by the convective boundary condition for the inside of the cavity was reapplied to the system as a Neumann boundary condition in order to satisfy the energy balance.

Radiative heat transfer was modeled using the net radiation method in the MOOSE modules. On the other hand, the view factors for the net radiation transfer method were produced using the ray tracing module [14]. This method assumes that the domain does not participate in heat transfer and heat exchanges between gray diffusive surfaces. The radiative heat flux for a surface is calculated using:

$$q'' = J_i - \sum_{j=1}^{N} F_{ij} J_j \tag{2}$$

where J_i and J_j are the radiosities at reference locations i and j, respectively, N is the total number of participating surfaces, and F_{ij} is the view factor between locations i and j. Further, the radiosity can be calculated using:

$$J_i = \epsilon_i \sigma T_i^4 + (1 - \epsilon_i) \sum_{j=1}^{N} F_{ij} J_j \tag{3}$$

There are three unknowns in the net radiation equations; however, there are only two equations to describe the system. The last equation depends on the boundary conditions of the modeled system. The system can be solved for either known surface temperatures or if the surface is adiabatic. This study will use the known surface temperature conditions.

Figure 14 presents the temperature contours produced by the heated cavity setup for Test #14 (forced convection, uniform low power 19.82 kW)[4]. The axial cut in the middle of the domain is taken to show temperature distribution within the cavity. The temperature profile shows consistent results with the expectations for the wall of the risers. The insulation material was added to the frame in order to reduce the amount of heat loss to the environment. The heat transfer coefficients and the bulk temperatures are shared in Table 4.

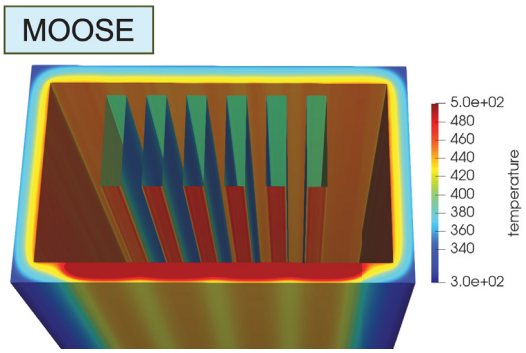

Figure 14. Temperature (K) contour of the heated cavity as axial cut in the middle of the domain.

Table 4. Heat transfer coefficient for the thermal model.

Heat Transfer Coefficient Data	Heat Transfer Coefficient $(W/(m^2K))$	Bulk Temperature (K)
Riser Ducts	25	323
Cavity Inside	6.14	420
Cavity Frame	5.82	295

For a more quantitative comparison between the experiment and MOOSE model, the axial temperature distributions for the front surface of the fourth riser were compared in Figure 15. The results were largely in agreement with each other, especially within the middle parts of the domain. However, certain inconsistencies observable closer to the lower and upper ends of the domain may have been caused by using a constant heat transfer coefficient and bulk temperature throughout the entire boundary. More sophisticated models for calculating heat transfer coefficients or modeling the fluid inside the cavity could improve the results.

3.3.2. Riser Ducts

The riser ducts are the main components of the RCCS designs. Their hydraulic characteristics have crucial effects on the performance of the RCCS. The riser ducts are responsible for a significant portion of the pressure drop in the RCCS, mainly caused by viscous loses. They have the hydraulic characteristics of the elongated ducts. The geometry is presented in Figure 16. The fluid properties are assumed constant, yielding the incompressible Navier-Stokes equations. The governing equations for the thermal-hydraulic model of riser ducts are:

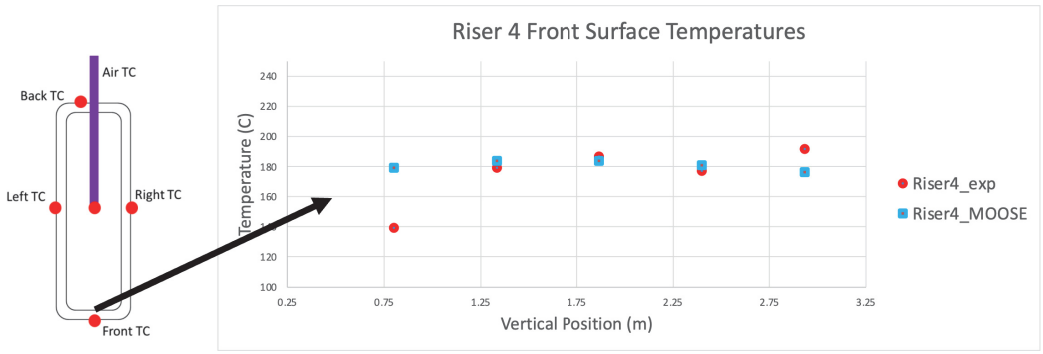

Figure 15. Forced convection test#14 temperature comparison between MOOSE and the RCCS experiment [4].

$$\nabla \cdot \mathbf{u} = 0 \tag{4a}$$

$$\rho \left(\frac{\partial \mathbf{u}}{\partial t} + \mathbf{u} \cdot \nabla \mathbf{u} \right) = -\nabla P + \nabla \cdot \tau + \rho \mathbf{f} \tag{4b}$$

$$\rho C_p \left(\frac{\partial T}{\partial t} + \mathbf{u} \cdot \nabla T \right) = \nabla \cdot (k \nabla T) + \dot{q} \tag{4c}$$

where t is time, $\mathbf{u}$ is the velocity vector, ρ is density, P is pressure, τ is the viscous stress tensor, $\mathbf{f}$ is a force vector, C_p is the isobaric specific heat capacity of the working fluid, T is temperature, and k is the thermal conductivity of the fluid. The properties are assumed to remain constant within the estimated temperature range of the system. The buoyancy force was modeled using the Boussinesq approximation, which assumes that the fluid density changes linearly with sufficiently small temperature differences in the system. Based on the reference facility, air is employed as the working fluid.

The riser ducts were simulated by using the NekRS code in tandem with the LES methodology. LES was employed for turbulence modeling, incorporating an explicit filter to replicate the dissipation effect of the subgrid scales. The Reynolds number (Re) for the system was estimated to be 15,615, indicating highly turbulent flow for the elongated duct geometry. The numerical models of the riser ducts were constructed based on the specifications outlined in the experimental report [4].

The case was intended to provide hydraulic verification and thermal-hydraulic validation of the numerical model constructed for the riser ducts. Therefore, the case is run twice: non-isothermal and isothermal cases. Figure 16 provides an overview of both the computational mesh and the employed boundary conditions. As indicated, a recycling region was implemented at the inlet to ensure a fully developed flow enters the riser ducts. The outflow treatment presented in Reference [20] was applied at the outlet to avoid the backflow issue. Lastly, the duct walls are assumed to have a no-slip condition. The Dirichlet boundary condition is applied for the energy equation. The values are derived from the experimental report for Test #14. [4]. To ensure the pressure profile was developed, the pressure drop along the fourth riser duct was calculated once two flow-through cycles had been completed after the initial start. The model setup and preferences are based on the previous study [21].

To verify the hydraulic numerical model, the same pressure drop was calculated using the following correlations: Bhatti and Shah [22], McAdams, and Colebrook [23]. The flow conditions satisfied the validity range of these correlations. The results are given in Table 5, which compares the pressure drop estimated by NekRS and the correlations. The difference between the simulation and correlation results is less than 5%, clearly indicating that the numerical model can predict the correct pressure profile. The comparison with the

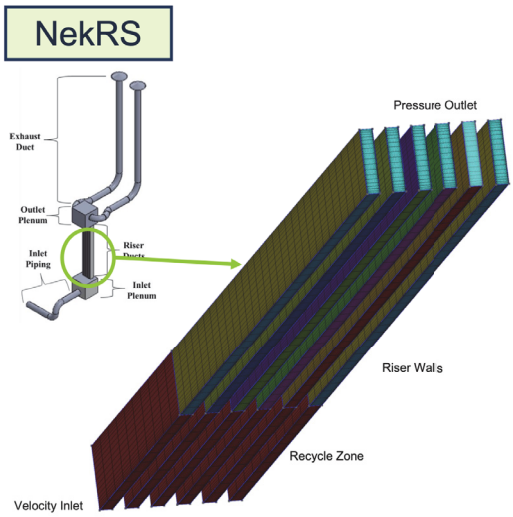

Figure 16. Riser ducts numerical model.

Bhatti and Shah correlation is more physical in this case since that specific correlation was established for elongated ducts, whereas the others were developed for pipe flow.

Table 5. Pressure comparison between NekRS hydraulic model and the literature.

Method	Pressure Drop (Pa)	Difference
NekRS	5.71	—
Bhatti & Shah	5.51	3.5%
McAdams	5.78	1.22%
Colebrook	5.98	4.64%

The nonisothermal case focused on the validation of the riser duct system, using the available experimental data. The energy equation was added to the system, and buoyancy was modeled using the Boussinesq approximation. The same Re number given in the previous section was again used here as well. To allow the temperature profile to develop, the simulation was run for a couple of flow-throughs before we began averaging the flow field. The temperature field statistics were then collected for two flow-throughs in order to estimate the averaged temperature profile.

Figure 17 presents the axial temperature profile obtained with NekRS using a fifth polynomial order solution and compares it to the experimental results. The experimental results show a reasonable match with the NekRS simulation. However, the simulation tends to overpredict the temperature after the midpoint of the channel. This discrepancy can be attributed to the data fitting used to derive the temperature boundary condition from the experiment. Future improvements in data fitting are expected to significantly enhance the accuracy of the results.

To demonstrate mesh convergence, the velocity profiles were compared across different mesh resolutions. The NekRS results were generated using third, fifth, and seventh polynomial orders. The velocity profiles for the fifth and seventh polynomial orders match well, indicating that the mesh has converged. The mesh convergence results are presented in Figure 18.

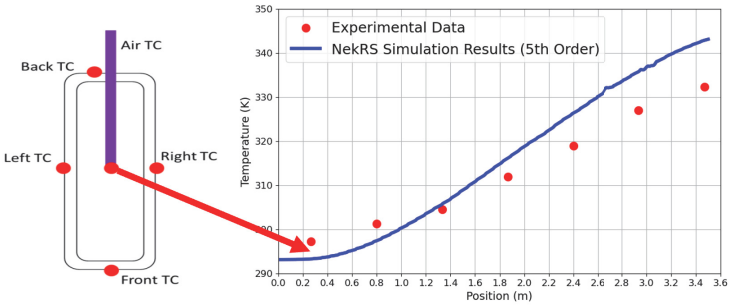

Figure 17. Temperature comparison of NekRS riser ducts and experimental results.

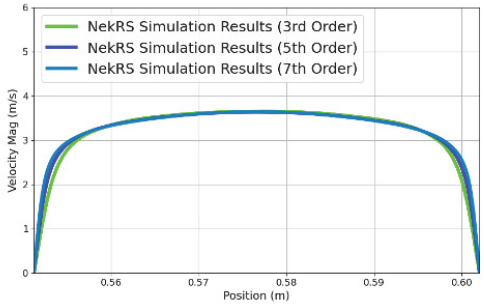

Figure 18. Comparison of velocity profiles for different mesh resolutions.

3.3.3. Multiphysics Test Cases

Figure 19 presents the multiphysics coupling strategy. The strategy consists of three domains to improve the stability of each nonlinear system: heat conduction, NekRS fluid flow (convection), and radiation (the solid, fluid, and radiation systems are shown in red, blue, and yellow, respectively, in Figure 19). These systems are coupled through their boundary conditions. Variables such as temperature and heat flux are transferred as fields using nearest-location transfer and their integrated values (total power) to maintain heat balance between the systems.

The time step starts with solving heat conduction in the solid domain and then proceeds to convection in the fluid flow. Finally, the radiative heat transfer between the surfaces of the fluid domain is solved. These time steps are repeated until the solution converges to a steady-state value. The fluid flow requires smaller time steps; therefore, for each solid heat conduction time step, several time steps are performed for fluid flow. This method is also called subcycling [24]. The boundary conditions of the fluid flow are dependent on radiative heat transfer, so the radiative heat transfer is calculated for each fluid time step.

The process begins by solving the heat conduction equation in the solid domain. The conductive heat flux and total power (integral of the conductive heat flux) are then transferred to the fluid region. The solid region receives the temperature at the interface as a boundary condition from the fluid region.

Next, the fluid simulation uses the heat flux as a boundary condition to solve fluid thermal-hydraulics and calculates the temperatures within the domain. The surface temperatures are then transferred to the radiation module, which simulates the radiative heat transfer using the net radiation method. The radiation module calculates the heat flux transfer between surfaces based on the surface temperatures from the fluid domain. Since the heat is transferred between the surfaces by radiative heat transfer, the convective heat flux is adjusted to maintain heat balance. This adjustment ensures that the total convective power equals the total

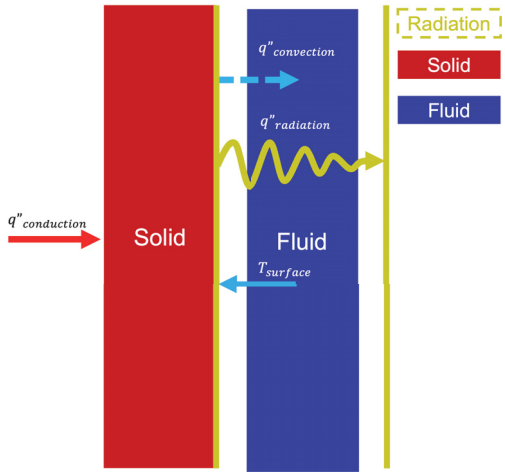

Figure 19. Multiphysics coupling strategy.

power (coming from conduction) minus the radiative power (integral of radiative heat flux).

The numerical setup for test cases can be seen in Figure 20. Solid and fluid domains are modeled as rectangular parallelepipeds. The dimensions of the solid domain are $0.25 \times 0.25 \times 1$ m, while the dimensions of the fluid domain are $0.25 \times 0.25 \times 1.25$ m. The additional height in the fluid region accounts for the inlet zone for fluid flow to improve stability. The fluid flow is laminar. The buoyancy force is not considered in this setup. The top and bottom walls in the solid region are assumed to be adiabatic. Heat is supplied as a Neumann boundary condition from the left side of the solid domain. The boundary conditions at the interface are Dirichlet, based on the surface temperatures from the fluid domain (the NekRS simulation). Velocity inlet and pressure outlet boundary conditions are used for the laminar fluid flow. The Reynold's number is calculated based on the hydraulic diameter of the square channel. The side walls have no-slip boundary conditions for the fluid. The properties of air are assumed to be constant under atmospheric conditions.

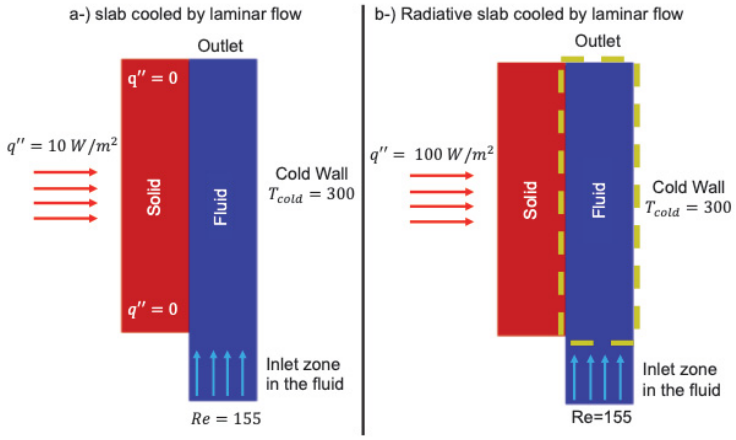

Figure 20. Numerical setups for test cases.

The first numerical model is the heated slab cooled by laminar flow presented in Figure 20.a. This test case aims to demonstrate Cardinal's capabilities for a conjugate heat transfer case. The heated solid is cooled by forced convection. The previously mentioned part of the multiphysics coupling strategy will be utilized for the first test case. Since there is no radiative heat transfer in the first case, only the transfers between heat

conduction and fluid flow will be modeled. The analytical heat conservation equation is derived to calculate the theoretical values:

$$q''_{\text{conduction}} = q''_{\text{convection}} = 10\,\text{W/m}^2 \tag{5a}$$

$$-k_{\text{solid}}\frac{T_{\text{hot}} - T_{\text{interface}}}{s_{\text{solid}}} = h(T_{\text{interface}} - T_{\text{bulk}}) = 10\,\text{W/m}^2 \tag{5b}$$

where T_{hot} represents the temperature of the left boundary in the solid, $T_{\text{interface}}$ is the temperature at the interface between the solid and fluid, and s_{solid} is the thickness of the solid domain, which is 0.25 m. Additionally, k_{solid} represents the thermal conductivity of the solid, set at 0.01 W/mK, while h is the heat transfer coefficient of laminar flow calculated from a constant Nusselt number for laminar flow (Nu=4.36). The heat balance equation is used to calculate the bulk temperature at the outlet:

$$Q_{Fluid} = \dot{m}C_p(T_{bulk,out} - T_{bulk,in}) \tag{6}$$

where Q_{Fluid} is the total energy transferred into fluid, $\dot{m}$ is the mass flow rate, and $T_{bulk,out}$ and $T_{bulk,in}$ is the outlet and inlet bulk temperatures, respectively.

The second canonical setup is the heated radiative slab cooled by a laminar flow. This test case includes more complicated physics than the first test case yet is simple enough to solve with hand calculations. The numerical setup can be seen in Figure 20.b. The radiative heat transfer is modeled in this numerical setup in addition to the first test case. Figure 20.b shows the radiative heat transfer boundaries as yellow dashed lines. The power value is increased for this case while the flow is kept in a laminar condition, which results in similar expected values in the fluid domain compared to the previous test case. This case aimed to be a radiative heat transfer dominated case because, in the RCCS scenario, radiative heat transfer is the significant form of heat transfer. The simplified form of the heat conservation equation is derived to calculate the theoretical values. The radiative heat transfer was added to the heat balance equations:

$$q''_{\text{conduction}} = q''_{\text{convection}} + q''_{\text{radiation}} = 100\,\text{W/m}^2 \tag{7a}$$

$$-k_{\text{solid}}\frac{T_{\text{hot}} - T_{\text{interface}}}{s_{\text{solid}}} = h(T_{\text{interface}} - T_{\text{bulk}}) \quad + \frac{\sigma\left(T^4_{\text{interface}} - T^4_{\text{cold}}\right)}{\frac{1}{\varepsilon_1} + \frac{1}{\varepsilon_2} - 1} = 100\,\text{W/m}^2 \tag{7b}$$

where σ is the Stefan-Boltzmann constant and ε_1 and ε_2 are the emissivity values of the surface of the interface and cold wall, which are set to 0.8.

The theoretical and simulation values are compared in Table 6 for each case. The values calculated from Cardinal simulations show good agreement with the theoretical values. The small differences can be attributed to assumptions made in the hand calculations, such as assuming a constant Nusselt number along the interface and not accounting for spatial effects. Hand calculations do not include spatial effects (2D or 3D) that can arise from a grid; instead, they assume the domain as two points (0D assumption). The last two columns show the power values calculated from the Cardinal simulations, showing how heat is distributed in each system.

A partial grid refinement study was conducted in the first test case (slab cooled by laminar flow) to ensure that the simulation results are not dependent on grid refinement. The number of divisions in the solid mesh was increased from 25 to 200 to observe the effect of grid refinement on the results. The results, shown in Figure 21, indicate that increasing the mesh divisions did not change the computed temperature values. The figure displays the outlet bulk temperature for various mesh divisions over time, demonstrating consistency across various refinements. One should note that the time in this figure represents the increase in the iterations since the analysis here is only focused on the steady-state results.

Table 6. Comparison of theoretical, cardinal values, and power distribution.

Slab Cooled by Laminar Flow				
Temperature	**Theoretical Value**	**Cardinal Value**	**Power**	**Value**
$T_{bulk,out}$	303 K	303 K	$Q_{Convection}$	2.5 W
$T_{interface}$	322 K	319 K	$Q_{Radiation}$	N/A
T_{hot}	572 K	569 K	$Q_{Conduction}$	2.5 W
Radiative Slab Cooled by Laminar Flow				
Temperature	**Theoretical Value**	**Cardinal Value**	**Power**	**Value**
$T_{bulk,out}$	303 K	303 K	$Q_{Convection}$	2.36 W
$T_{interface}$	321 K	317 K	$Q_{Radiation}$	22.64 W
T_{hot}	2820 K	2817 K	$Q_{Conduction}$	25 W

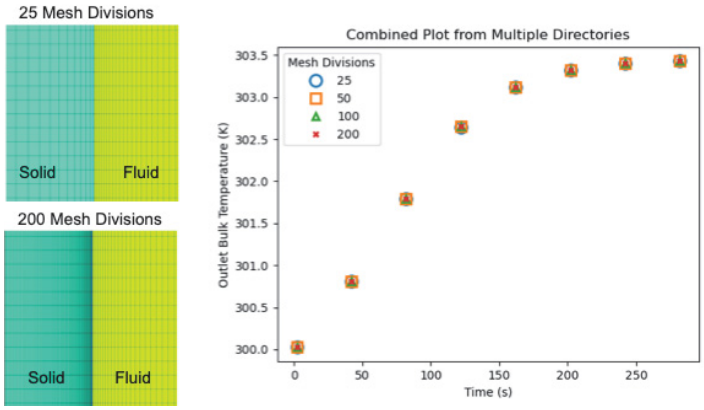

Figure 21. Grid independence study for multiphysics coupling approach.

3.4. RCCS Thermal-Hydraulics Results

This section presents the results for the RCCS cooling system based on the riser ducts model described previously. This model is more complex than the canonical setup, featuring realistic RCCS geometry and incorporating the heat conservation equation in the fluid flow. This initial model is designed to address the thermal-hydraulic aspects of the system. Temperatures at the riser duct walls are imposed as Dirichlet boundary conditions derived from experiments [4]. The final model will include the multiphysics strategy previously tested. Figure 13 shows the numerical model alongside a sketch of the experimental facility. The study's initial focus is to ensure accurate modeling of the inlet plenum, riser ducts, and outlet plenum. Therefore, this model does not yet include the exhaust ducts or all of the inlet piping.

This model contains more than 1.7 million elements, corresponding to 2.13×10^8 grid points for a fourth-order polynomial solution in NekRS. The preliminary results show turbulent jet interactions in the outlet plenum. The flow patterns observed here can significantly affect the performance of the RCCS. The following study [25] also observed that turbulent jet interactions can impact the flow characteristics. The experimental report states that the flow reversal happened in exhaust ducts because of flow instabilities for natural convection experiments [4]. The turbulent jet interactions can possibly be a contributor to the flow

instabilities for the system. The instantaneous temperature at the outlet plenum is shown in Figure 22. The flow enters from the riser ducts, mixes in the outlet plenum, and then discharges through the exhaust ducts [26]. The results are being post-processed to obtain averaged temperature, velocity, and pressure fields. The temperature field will be compared to experimental data. Additionally, the model will be run with a higher polynomial order to ensure grid convergence of the results. The mesh analysis will include a comparison of grid length to Taylor's microscale to meet the length scale requirements for the LES methodology.

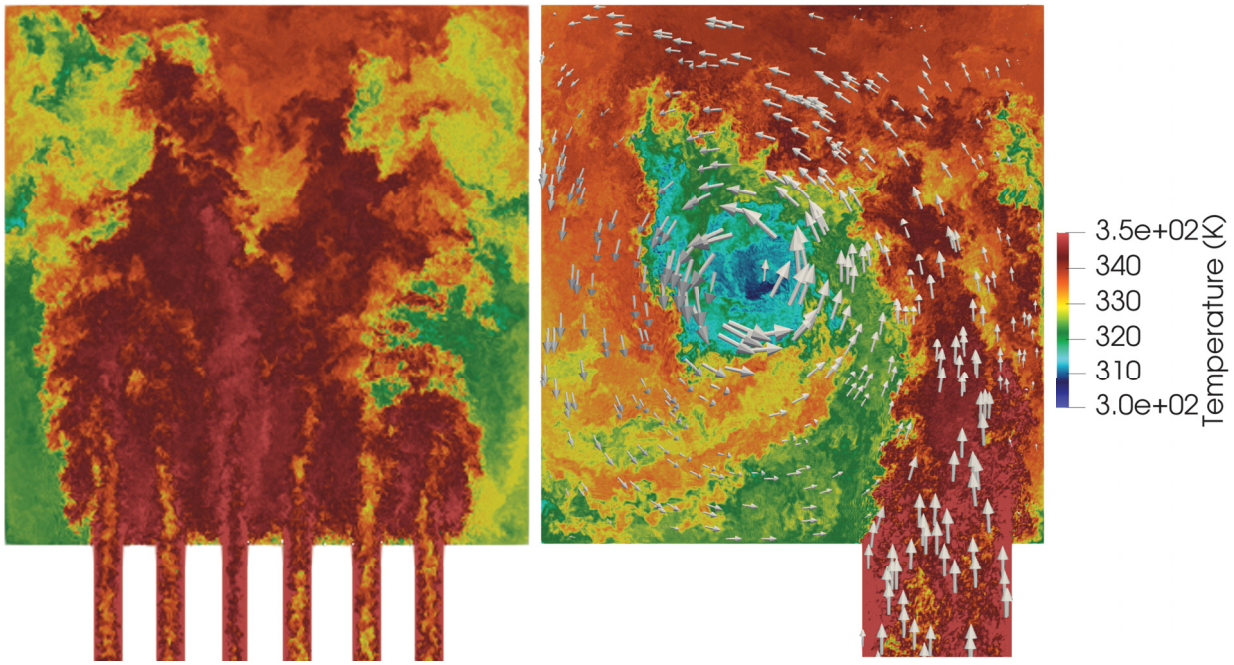

Figure 22. Instantaneous temperature at outlet plenum: left (front view) and right (side view). White arrows were added to the side view to show the flow direction in the outlet plenum.

4. PEBBLE-BED HOT GAS MIXING IN THE LOWER PLENUM EXPERIMENT MODELING AND VALIDATION

The path of coolant flow through an HTGR tends to be complex in both space and time. The random packing of the pebble-bed core, bypass flow through reflector blocks, and the complex geometry of other system components make understanding of the flow and heat transfer in these systems difficult. Many steam generators used for power conversion in HTGR's require a fairly uniform temperature of the heated primary circuit to operate efficiently and maintain component reliability [27]. The lower plenum in an HTGR is therefore designed to enhance the mixing of hot and cold streams of flow from the core and bypass regions to minimize the temperature differential of the fluid that enters the steam generator. The lower plenum, like many other components in an HTGR, tends to have a complex structure consisting of many channels, plenums, and mixing regions. Simulations of the lower plenum can therefore be used to help guide lower plenum design to ensure that the flow is sufficiently mixed prior to entering the steam generator.

High-fidelity simulations of these flows with LES or Direct Numerical Simulation (DNS) are possible but are typically incredibly expensive due to the grid resolution necessary to resolve the intricate geometries found in HTGRs. Experimental measurements in these systems are also possible but difficult due to system complexity. Therefore, many researchers instead rely on lower-order modeling-based approaches, such as 3D Reynolds-Averaged Navier Stokes (RANS) models, 2D porous media models, or 1D system models. The

intricate structures in the lower plenum of an HTGR, however, introduce strong mixing and other turbulent effects that are not easy to reproduce with these modeling-based approaches. Verification and validation of available CFD modeling approaches is therefore highly desired to ensure that cheap and efficient CFD models are capable of accurately reproducing the physics seen in real-world lower plenum designs.

Researchers at INET have performed experiments related to the mixing in the lower plenum of an HTGR [28]. Their facility represents a scaled-down version of the HTR-PM reactor at a 1:2.5 scale, and measurements of flow velocity, pressure, and temperature were taken at several locations in the geometry.

This section focuses on the use of the INET experimental measurements to validate CFD models of mixing in the lower plenum of an HTGR. The experimental facility is described in greater detail in Section 4.2, followed by an introduction to the current modeling approach and preliminary results in Section 4.3.

4.1. HTGR Lower Plenum Design

The lower plenum in an HTGR typically consists of the bottom graphite reflector, the hot gas chamber, and the hot gas duct. Flow enters the bottom graphite reflector from the top, where it passes through a series of channels that are carved through the graphite. These channels are connected at several locations with disk-shaped cavities, called cross channels. After passing through the bottom graphite reflector, the flow then enters the hot gas chamber. Some flow may also flow directly from the core to the hot gas chamber through the pebble outlet chute. In the hot gas chamber, petal-shaped blocks support the weight of the structure above. Flow from the channels in the bottom graphite reflector enters the gaps between these petal-shaped blocks. These gaps include arc-shaped features that are intended to promote the generation of eddies to enhance flow mixing. Flow may also bypass a large region of the core and the entire lower mixing structure and pass straight from the core to the hot gas chamber through bypass channels. This is particularly problematic for the HTGR design, as this introduces largely unmixed cold air into the hot gas chamber. The coolant then flows outward through the gaps into the main cavity of the hot gas chamber, where it then exits through the hot gas duct. A diagram of the lower reflector and hot gas chamber is in Figure 23.

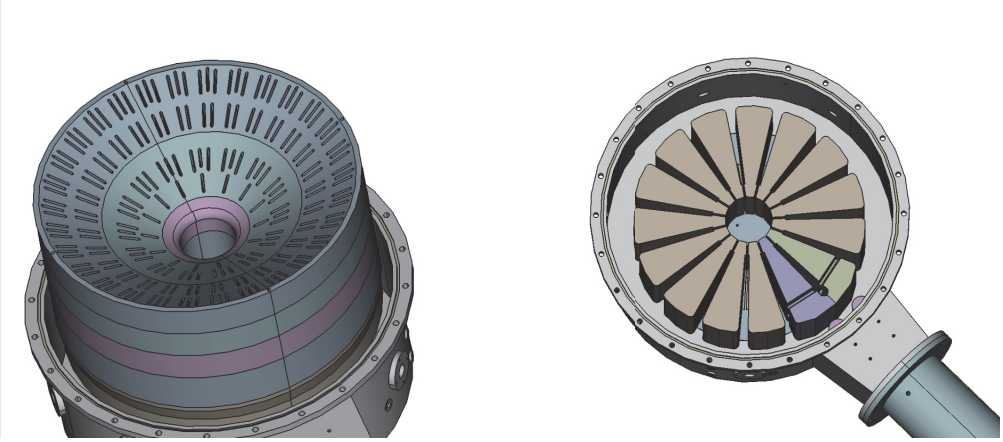

Figure 23. Lower mixing structure bottom graphite reflector with cross channels (left) and lower mixing structure hot gas chamber with petal blocks (right).

4.2. Lower Plenum Mixing Experimental Facility

The lower plenum mixing experimental facility at INET is a 1:2.5 recreation of the lower plenum structure in the HTR-PM [28]. The system is designed to preserve the Reynolds number, Prandtl number, and relative temperature difference found in the HTR-PM. The experimental facility uses air at atmospheric pressure as

the working fluid. This provides a Prandtl number within reasonable match of the helium in the HTR-PM. The air enters the top of the facility through one hot gas inlet in the center and four cold gas inlets around the perimeter. A divider in the inlet tank prevents these five streams from mixing prior to entering the lower plenum structure. The facility is designed to operate at a total gas Mass Flow Rate (MFR) of 4 kg/s, with the capability to operate up to 5 kg/s. The cold air in the experimental facility is at room temperature, with a temperature difference of up to 100 K between the inlet cold and hot gas streams. The air enters the inlet tank where it then progresses through the bottom reflector and hot gas chamber to mix before exiting through the hot gas duct. A picture of the experimental facility is in Figure 24.

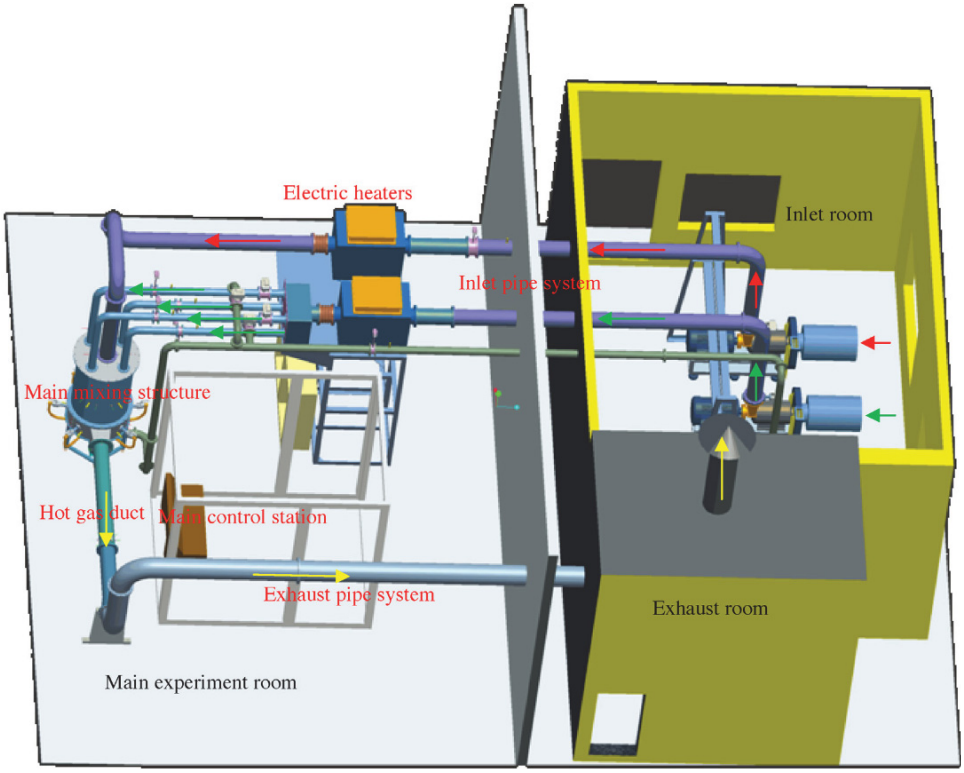

Figure 24. Picture of the lower plenum mixing facility at INET, retrieved from Reference [28].

4.3. Computational Model Of The Lower Plenum Mixing Facility

Initial work has been focused on the creation of a numerical model of the INET lower plenum mixing facility. A Computer-aided design (CAD) model for the fluid region was created based on the provided geometric information from INET.

This model was then imported into STAR-CCM+ to prepare for mesh generation. STAR-CCM's automated mesh generator was used to create the mesh for the fluid domain. A visualization of the geometry with labeled boundary conditions is shown in Figure 25. These simulations are targeting wall-modeled RANS, and the mesh is designed to target a wall y+ value between 30 and 200. An example of the current mesh is shown in Figure 26. Initial simulations have focused on the experiment with the conditions provided in Table 7.

The simulation is then run until a steady condition is achieved. Visualizations of the fluid velocity and temperature fields are shown in Figure 27 and Figure 28. Work is currently being performed to investigate the sensitivity of the results to the mesh resolution. Simulations will then be performed of several experiments at

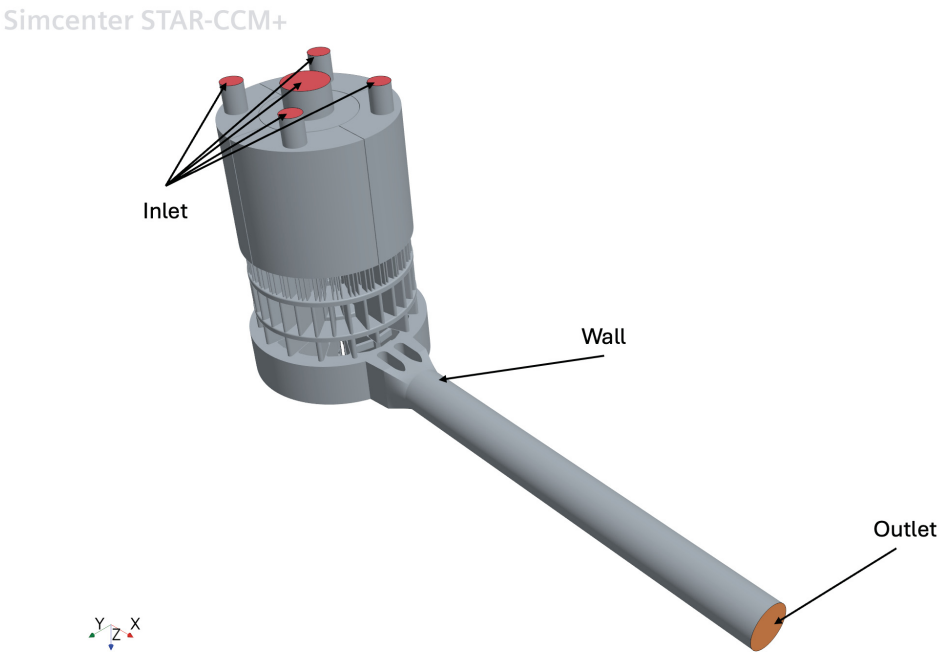

Figure 25. Geometry of the lower plenum mixing facility fluid domain with labeled boundary conditions.

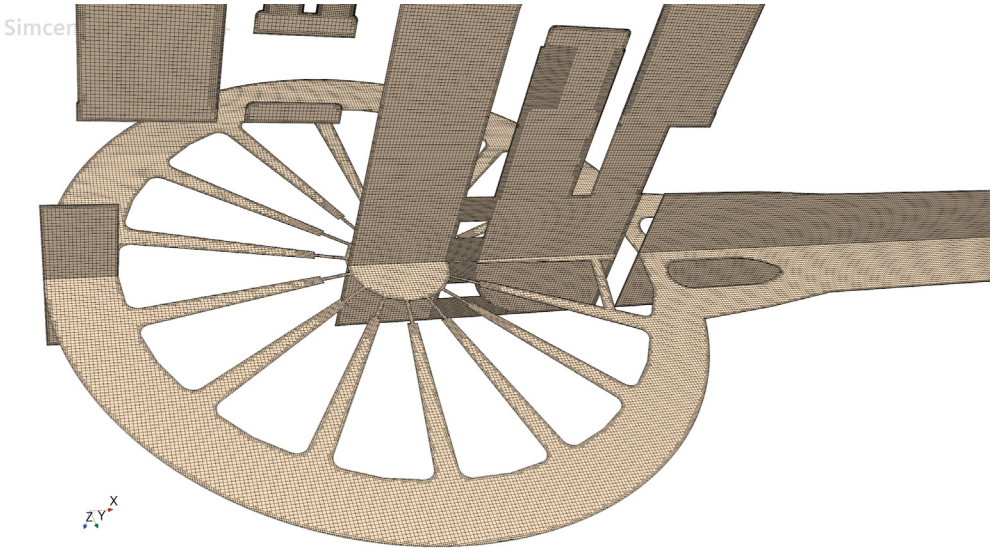

Figure 26. Slice of the fluid mesh for the RANS simulation of the lower plenum mixing facility.

different flow rates and inlet temperature differences to quantify the capability of RANS models to accurately predict the mixing in the lower plenum.

Table 7. Simulation input parameters for the initial simulation of the lower plenum mixing experiment.

Parameter	Value
Hot Gas MFR	1.1 kg/s
Hot Gas Temperature	393 K
Cold Gas MFR	1.1 kg/s
Cold Gas Temperature	293 K

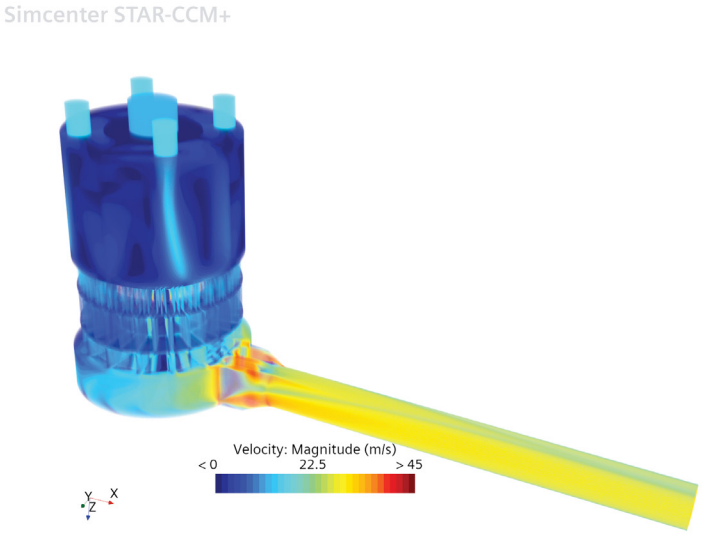

Figure 27. Visualization of the preliminary velocity field result for the RANS simulation of the lower plenum mixing facility.

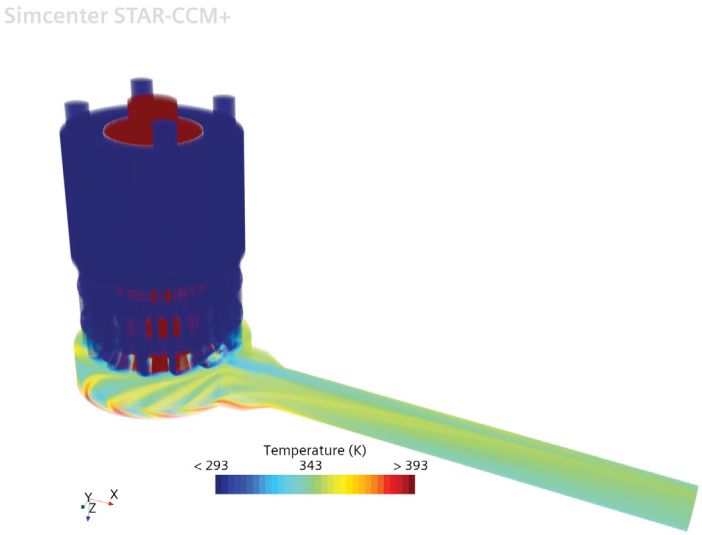

Figure 28. Visualization of the preliminary temperature field result for the RANS simulation of the lower plenum mixing facility.

5. CONCLUSIONS

Updating and reviewing the PIRTs is crucial for deepening our understanding of HTGR scenarios and phenomena. The new template being developed will soon facilitate comparisons with other countries that have licensed HTGRs, enhancing international insights. Moreover, the neutronic validation of the AGR-1 and AGR-2 benchmarks has demonstrated excellent agreement between experimental and calculated values, confirming the reliability of these benchmarks to confirm the maturity of our tools and methodologies.

In the field of CFD, high-fidelity simulations of the RCCS using NekRS and MOOSE have been validated against experimental data, confirming the accuracy of these numerical models in predicting real-world behavior. Furthermore, the capabilities of the tools have been assessed for modeling the complex geometry of the lower plenum in HTR-PM, with preliminary results showing promising agreement with the provided data.

These activities will be presented at the next VHTR-CMVB meeting this fall and will continue throughout Fiscal Year 2025, involving further data comparisons with models and expanding to other experiments.

6. REFERENCES

[1] Sterbentz, J. W. and Cogliati, J. J., AGR-1 Depletion Benchmark. Technical Report INL/EXT-18-45840, Idaho National Lab. (INL) (2018).

[2] Kulesza, J. A., Adams, T. R., Armstrong, J. C., Bolding, S. R., Brown, F. B., Bull, J. S., Burke, T. P., Clark, A. R., Forster, III, R. A., Giron, J. F., Grieve, T. S., Josey, C. J., Martz, R. L., McKinney, G. W., Pearson, E. J., Rising, M. E., Solomon, Jr., C. J., Swaminarayan, S., Trahan, T. J., Wilson, S. C., and Zukaitis, A. J., MCNP® Code Version 6.3.0 Theory & User Manual. Technical Report LA-UR-22-30006, Rev. 1, Los Alamos National Laboratory Los Alamos, NM, USA (September, 2022).

[3] Ryskamp, J. M., Gorski, E. J., Harvego, E. A., Khericha, S. T., and Beitel, G. A., New Generation Nuclear Plant – High Level Functions and Requirements. Technical Report INEEL/EXT-03-01163, Idaho National Laboratory (9, 2003).

[4] Corradini, M., Anderson, M., Muci, M., Hassan, Y., Dominguez, A., Tokuhiro, A., and Hamman, K., Thermal-Hydraulic Analysis of an Experimental Reactor Cavity Cooling System with Air. Part I: Experiments; Part II: Separate Effects Tests and Modeling. Technical Report DOE/NEUP-11-3079; 11-3079, Univ. of Wisconsin, Madison (10, 2014).

[5] Lisowski, D. D., Gerardi, C. D., Hu, R., Kilsdonk, D. J., Bremer, N. C., Lomperski, S. W., Kraus, A. R., Bucknor, M. D., and Farmer, M. T., Water NSTF Design, Instrumentation, and Test Planning. Technical Report ANL-ART-98, Argonne National Laboratory (8, 2017).

[6] Lisowski, D. D., Gerardi, C. D., Kilsdonk, D. J., Bremer, N. C., Lomperski, S. W., Hu, R., Kraus, A. R., Bucknor, M. D., Lv, Q., Lee, T., and Farmer, M. T., Final Project Report on RCCS Testing with Air-based NSTF. Technical Report ANL-ART-47, Argonne National Laboratory (8, 2016).

[7] Hu, R., Kraus, A., Bucknor, M., Lv, Q., and Lisowski, D., Final Project Report on Computational Modeling and Analysis of Air-Based NSTF. Technical Report ANL-ART-46, Argonne National Laboratory (6, 2016).

[8] Freile, R., Tano, M., Balestra, P., Schunert, S., and Kimber, M. (2021) Improved natural convection heat transfer correlations for reactor cavity cooling systems of high-temperature gas-cooled reactors: From computational fluid dynamics to Pronghorn. *Annals of Nuclear Energy,* **163**, 108547.

[9] Kim, C. S., Lisowski, D., Bae, Y. Y., Kim, J. H., and Lee, S. N. (2021) Comparative study with two reduced test facilities for air-cooled RCCS scaling law. *Nuclear Engineering and Design,* **380**, 111276.

[10] Kim, J.-H., Bae, Y.-Y., Kim, C.-S., Hong, S.-D., and Kim, M.-H. (2015) The test results of the NACEF RCCS test facility. In *Transactions of the Korean Nuclear Society Spring Meeting* pp. 7–8.

[11] Lomperski, S., Pointer, W. D., Tzanos, C. P., Wei, T. Y., and Kraus, A. R., Generation IV nuclear energy system initiative; air-cooled option RCCS studies and NSTF preparation. Technical Report ANL-GenIV-179, Argonne National Laboratory (11, 2012).

[12] Hu, R., Lisowski, D. D., Bucknor, M. D., Kraus, A. R., and Lv, Q. (2018) Ambient and building condition effects modeling of air-cooled natural circulation systems. *Applied Thermal Engineering,* **137**, 23–31.

[13] Shin, D.-H., Kim, S.-Y., Kim, C. S., Park, G.-C., and Cho, H. K. (07, 2018) Study on the Turbulent Mixed Convection Phenomena Inside the Air-Cooled RCCS Riser. In Vol. Volume 6B: Thermal-Hydraulics and Safety Analyses of International Conference on Nuclear Engineering, p. V06BT08A029.

[14] Lindsay, A. D., Gaston, D. R., Permann, C. J., Miller, J. M., Andrš, D., Slaughter, A. E., Kong, F., Hansel, J., Carlsen, R. W., Icenhour, C., Harbour, L., Giudicelli, G. L., Stogner, R. H., German, P., Badger, J., Biswas, S., Chapuis, L., Green, C., Hales, J., Hu, T., Jiang, W., Jung, Y. S., Matthews, C., Miao, Y., Novak, A., Peterson, J. W., Prince, Z. M., Rovinelli, A., Schunert, S., Schwen, D., Spencer, B. W., Veeraraghavan, S., Recuero, A., Yushu, D., Wang, Y., Wilkins, A., and Wong, C. (2022) 2.0 - MOOSE: Enabling massively parallel multiphysics simulation. *SoftwareX,* **20**, 101202.

[15] Weiss, A. G., Zaidan, L. J., Bani Ahmad, M. H., Abdoelatef, M. G., Peterson, J. W., Lindsay, A. D., Kong, F., Ahmed, K., and Kimber, M. L. (6, 2022) Characterization of the Finite Element Computational Fluid Dynamics Capabilities in the Multiphysics Object Oriented Simulation Environment. *Journal of Nuclear Engineering and Radiation Science,* **9**(2).

[16] Fischer, P., Kerkemeier, S., Min, M., Lan, Y.-H., Phillips, M., Rathnayake, T., Merzari, E., Tomboulides, A., Karakus, A., Chalmers, N., and Warburton, T. (2022) NekRS, a GPU-accelerated spectral element Navier–Stokes solver. *Parallel Computing,* **114**, 102982.

[17] Merzari, E., Rahaman, R., Min, M., and Fischer, P. (July, 2018) Performance Analysis of Nek5000 for Single-Assembly Calculations. In V002T09A031 Vol. Volume 2 of Fluids Engineering Division Summer Meeting, .

[18] Novak, A., Andrs, D., Shriwise, P., Fang, J., Yuan, H., Shaver, D., Merzari, E., Romano, P., and Martineau, R. (2022) Coupled Monte Carlo and Thermal-Fluid Modeling of High Temperature Gas Reactors Using Cardinal. *Annals of Nuclear Energy,* **177**, 109310.

[19] MacGregor, R. K. and Emery, A. F. (08, 1969) Free Convection Through Vertical Plane Layers—Moderate and High Prandtl Number Fluids. *Journal of Heat Transfer,* **91**(3), 391–401.

[20] Dong, S. and Shen, J. (2015) A pressure correction scheme for generalized form of energy-stable open boundary conditions for incompressible flows. *Journal of Computational Physics,* **291**, 254–278.

[21] Okyay, S., Coppo Leite, V., Merzari, E., Balestra, P., and Strydom, G. (2024) High-Fidelity Simulations of an Air-cooled Reactor Cavity Cooling System. In *Pacific Basin Nuclear Conference* Idaho Falls: .

[22] Bhatti, M. (1987) Turbulent and transition flow convective heat transfer in ducts. *Handbook of single-phase convective heat transfer,*.

[23] Todreas, N., Kazimi, M., and Massoud, M. (2021) Nuclear Systems Volume II: Elements of Thermal Hydraulic Design, CRC Press, .

[24] Novak, A. J., Shriwise, P., Romano, P. K., Rahaman, R., Merzari, E., and Gaston, D. (2023) Coupled Monte Carlo Transport and Conjugate Heat Transfer for Wire-Wrapped Bundles Within the MOOSE Framework. *Nuclear Science and Engineering,* **197**(10), 2561–2584.

[25] Merzari, E., Coppo Leite, V., Fang, J., Shaver, D., Min, M., Kerkemeier, S., Fischer, P., and Tomboulides, A. (02, 2024) Energy Exascale Computational Fluid Dynamics Simulations With the Spectral Element Method. *Journal of Fluids Engineering,* **146**(4), 041105.

[26] Okyay, S., Coppo Leite, V., Merzari, E., Balestra, P., and Strydom, G. (2024) Multi-physics Modeling of Radiative Heat Transfer and Fluid Flow for the Reactor Cavity Cooling System. In *Advances in Thermal Hydraulics (ATH 2024)* Orlando: .

[27] Damm, G. and Wehrlein, R. (1992) Simulation tests for temperature mixing in a core bottom model of the HTR-Module. *Nuclear Engineering and Design,* **137**, 97–105.

[28] Zhou, Y., Hao, P., Li, F., Shi, L., He, F., Dong, Y., and Zhang, Z. (2016) Experiment study on thermal mixing performance of HTR-PM reactor outlet. *Nuclear Engineering and Design,* **306**, 186–191.